Infrared Imaging of Sub-retinal Structures in the Human Ocular Fundus

ANN E. ELSNER,*†‡ STEPHEN A. BURNS,*† JOHN J. WEITER,*† FRANCOIS C. DELORI*†

The interaction of infrared light with the human ocular fundus, particularly sub-retinal structures, was studied *in vivo*. Visible and infra-red wavelengths and a scanning laser ophthalmoscope were used to acquire digital images of the human fundus. The contrast and reflectance of selected retinal and sub-retinal features were computed for a series of wavelengths or modes of imaging. Near infrared light provides better visibility than visible light for sub-retinal features. Sub-retinal deposits appear light and thickened; the optic nerve head, retinal vessels, and choroidal vessels appear dark. Contrast and visibility of features increases with increasing wavelength from 795 to 895 nm. Optimizing the mode of imaging improves the visibility of some structures. This new quantitative basis for near infrared imaging techniques can be applied to a wide range of imaging modalities for the study of pathophysiology and treatment in diseases affecting the retinal pigment epithelium and Bruch's membrane, such as age-related macular degeneration.

Pathology   Pigment epithelium   Infrared   Imaging   Scanning laser ophthalmoscope

INTRODUCTION

Sub-retinal or pre-clinical pathology is difficult to observe and quantify *in vivo*. Sub-retinal pathology is a hallmark in age-related macular (AMD), one of the chief causes of visual loss in the United States in elderly adults (Leibowitz, Kruger, Maunder, Milton, Kini, Kahn, Mickerson, Pool, Colton, Ganley, Loewenstein & Dawber, 1980). Histopathological studies of human eyes indicate that there is a deposition of material in the layers beneath the retina. There is diffuse thickening within Bruch's membrane or between the retinal pigment epithelium (rpe) and the basement membrane, as well as focal deposits (drusen) within Bruch's membrane (Feeney-Burns & Ellersieck, 1985; Sarks, Sarks & Killingsworth, 1988; van der Schaft, Mooy, de Bruijn, Oron, Mulder & de Jong, 1992; Green and Enger, 1993; Bressler, Silva, Bressler, Fine & Green, 1994). There is also a redistribution of the melanin in the rpe, as sick cells shed their melanin and neighboring cells take it up (Boulton, Docchio, Dayhaw-Barker, Ramponi & Cubeddu, 1990). Choroidal new vessels can form, which presents a severe risk for vision loss. Neither small deposits (< 25 µm) nor early changes are observable with standard clinical methods.

*Schepens Eye Research Institute, 20 Staniford Street, Boston, MA 02114, U.S.A.
†Department of Ophthalmology, Harvard University, 243 Charles Street, Boston MA 02114, U.S.A.
‡To whom correspondence should be addressed, at Schepens Eye Research Institute.

Potential pathological fundus structures can be quantified with a scanning laser ophthalmoscope (SLO) (Webb, Hughes & Delori, 1987; Webb & Delori, 1988; Elsner, Burns, Hughes & Webb, 1992a). Near infrared imaging is well-suited for investigating sub-retinal structures (Elsner, Burns & Webb, 1988; Elsner, Burns, Hughes & Webb, 1990). With an SLO, initial infrared images (790 nm) revealed details of most fundus features (Webb & Delori, 1988; Elsner *et al.*, 1988). Contemporary infrared images with a fundus camera reveal only large or highly pigmented structures (Bonin, Faunay & Fauconnier, 1990). Quantitative comparison of infrared images from an SLO and a fundus camera showed that only with the SLO were the contrasts for retinal veins and arteries similar to those obtained with shorter wavelength light (Elsner *et al.*, 1990). The failure of the fundus camera to provide useful images in infrared light can be attributed to the failure to separate reflected and scattered light, since infrared light is absorbed less than visible light, and thus may scatter over longer distances.

Infrared imaging detects pathology (Elsner *et al.*, 1990; Elsner, Burns, Kreitz & Weiter, 1991; Scheider, Kaboth & Neuhauser, 1992), despite the presence of hemorrhage or cataract (Elsner, Jalkh & Weiter, 1993), that may be undetected in *in vivo* angiographic dye studies. In this paper we provide the first step for a model of the interaction of infrared light with human fundus tissue. First, the spectral characteristics of the major pigments of the human fundus are compared with reflectance spectra, showing that confocal images are primarily determined by reflected light. Next images from an SLO are compared both qualitatively

and quantitatively to show changes across experimental conditions for a series of wavelengths and imaging modes.

Wavelength effects in the imaging of the human fundus: comparison of in vivo reflectance with ex vivo absorption

The layers of the human fundus contain a variety of absorbing, reflecting, and scattering materials, which differ significantly across individuals (van Norren & Tiemeijer, 1986; Delori & Pflibsen, 1989). Absorbing substances, such as blood and melanin, greatly influence the information in fundus images in visible wavelength illumination (Delori, Gragoudas, Francisco & Pruett, 1977; Ducrey, Delori & Gragoudas, 1979). We extended these results to near infrared illumination.

The *in vivo* (double-pass) reflectance of the fundus was measured as a function of wavelength from 400–1100 nm, using the method of Delori and Pflibsen (1989). Reflectance spectra were obtained for two subjects, following explanation of procedure and obtaining consent; one was lightly pigmented (male, 37 yr) and one darkly pigmented (female, 41 yr). Subjects had dilated pupils.

The *in vivo* reflectance of the human ocular fundus is much higher, about 1 log unit, with near infrared illumination (e.g. 830 nm) than with short wavelength illumination (450 nm) [Fig. 1(a)]. Fundus reflectance increases with increasing wavelength in a non-monotonic way. In the darkly pigmented fundus, because of abundant melanin in the choroid, the reflectance increases more gradually with increasing wavelength for 500–650 nm than in the lightly pigmented fundus. In contrast, the reflectance spectra are similar in shape for near infrared illumination (longer than about 800 nm).

For comparison the major absorbing substances, for the human ocular fundus are plotted in Fig. 1(b), with the exception of macular pigment, which decreases for wavelengths greater than 460 nm. The *ex vivo* absorption spectra were compiled from several studies by F.D., and the wavelength-dependent absorption computed for the 4 primary ocular pigments. Melanin was computed from the average of several studies, then plotted as the extinction coefficient (Gabel, Birngruber & Hillenkamp, 1978; Wolbarsht, Walsh & George, 1981; Menon, Persad, Haberman, Kurian & Basu, 1982). Blood components, both oxygenated hemoglobin and hemoglobin (Assendelft, 1970), were scaled to represent a column 100 μm thick. Water (Sullivan, 1963) and lens density for a 40-yr-old human (Pokorny, Smith & Lutze, 1987) are also shown on an absorption scale. Macular pigment (not shown), which masks the underlying fundus layers in the foveal region to a variable extent across individuals, also has peak absorption in the short wavelengths and minimal effect in infrared light (not shown) (Wyszecki & Stiles, 1982a; Snodderly, Brown, Delori & Auran, 1984). Although plotted together for compactness, the absolute absorptions of the pigments cannot be compared to each other, since they depend upon the concentration of each pigment.

The non-monotonically increasing *in vivo* reflectance spectra are consistent with the *ex vivo* absorption spectra. That the agreement is incomplete results from the reflectance spectra representing the cumulative effects of several sources, in both the anterior and posterior segments, of absorption, reflectance, and scattering. For about 500–650 nm, there are non-monotonic changes in both the *in vivo* and *ex vivo* spectra that correspond to the major absorbing components of blood. For 700–900 nm, oxygenated hemoglobin (choroidal blood) increases in absorption monotonically, whereas melanin continues to decrease in absorption in this spectral range. At about 950–1050 nm, there is a large decrease in the *in vivo* spectra that corresponds to the increase in water absorption.

Infrared illumination may improve imaging of subretinal features, given the potential advantages that less light should be needed to produce an image and that increased penetration through the fundus could provide information from deeper layers [Fig. 2(A)]. In previous studies, information concerning the deeper layers was
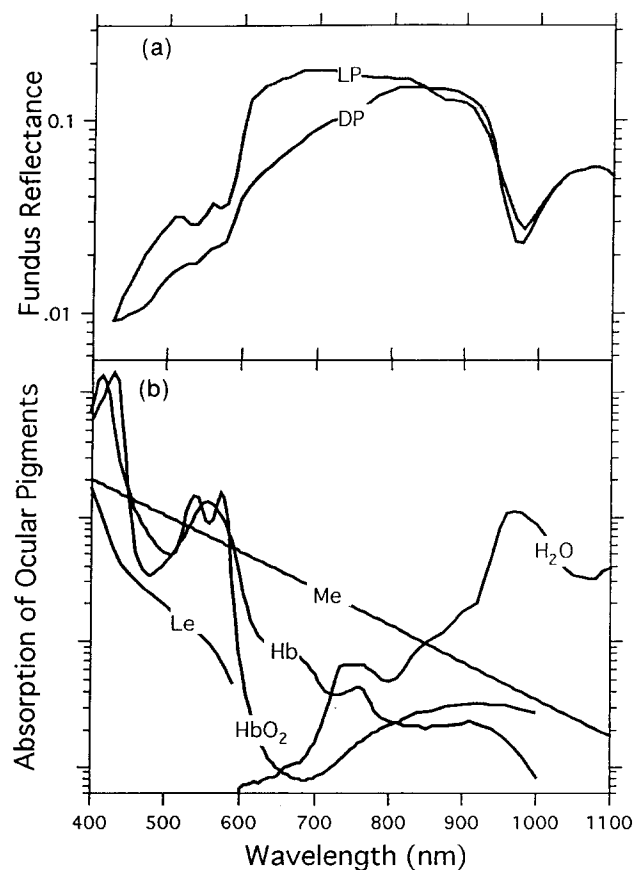

FIGURE 1. The effects of wavelength on imaging the human fundus with a confocal instrument. (a) The *in vivo* reflectance (double-pass) of the fundus as a function of wavelength for two subjects: (DP)—darkly pigmented subject, (LP)—lightly pigmented subject. (b) Calculated wavelength dependence of the absorptions of the 4 primary ocular pigments: Me, melanin, computed from the average of 4 studies, plotted as extinction coefficient; HbO$_2$, oxygenated hemoglobin and Hb, hemoglobin scaled to represent a column 100 μm thick, H$_2$O, water, and Le lens density for a 40-yr-old human (after Snodderly *et al.*, 1984).

(A)

Confocal
Apertures

B G IR

Choroid Retina
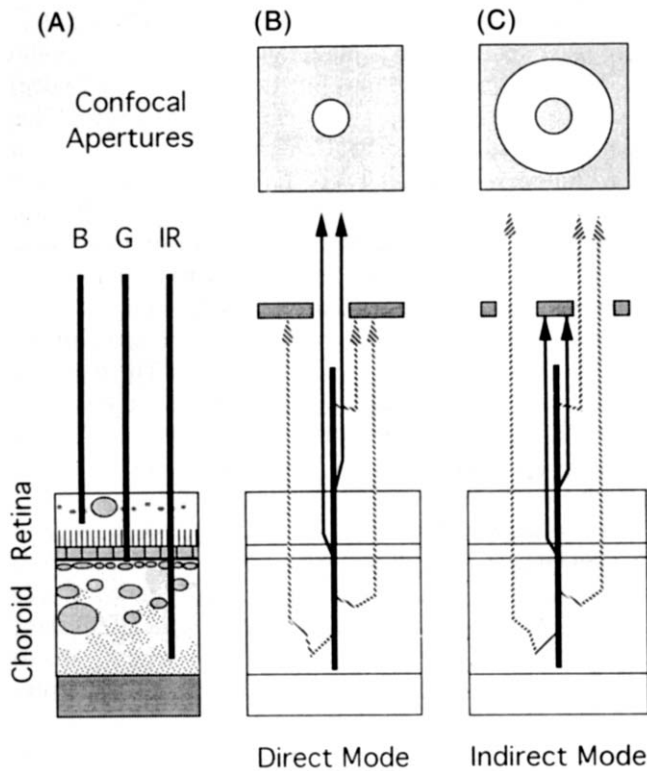
(B)

(C)

Direct Mode   Indirect Mode

FIGURE 2. Schematic diagrams of the effects of wavelength and confocal aperture on the visibility of the fundus features. Dark vertical lines represent the instantaneous position of the scanned, focused laser illumination. (A) With increasing wavelength, light penetrates more deeply into retinal and choroidal structures: infrared (IR) light more deeply than middle wavelength visible (G or green), in turn more than short wavelength (B or blue) light. (B) Direct mode imaging with a circular aperture. The aperture (gray rectangles) passes light returning from the plane of focus (solid arrows) and minimizes light returning from the sample to the detector from planes not in focus, e.g. ocular media or deeper layers, (stippled arrows) or light that is scattered laterally. This produces high contrast images of features that reflect or backscatter. (C) Indirect mode imaging with an annular aperture, analogous to dark field microscopy. Increasing the diameter of the central stop of the aperture (gray rectangles) decreases the reflecting or backscattering light from the plane of focus (dark arrows) and passes light that is from other planes of focus or that is laterally scattered (stippled arrows). For longer wavelength light that can penetrate deeply, structures in the rpe or choroid may be back- or side-illuminated.

difficult to extract with short wavelength illumination (Delori et al., 1977), especially for darkly pigmented subjects. This is consistent with high absorption of short wavelength light by the blood and melanin in these layers. With long wavelength visible illumination, there is still significant absorption by choroidal blood (Delori & Pflibsen, 1989). Another potential advantage of infrared illumination is that there is less difference in total reflection between subjects for near infrared wavelengths than for shorter wavelengths, thus minimizing the confounding effects of intra-individual differences in ocular pigmentation. However, more light does not necessarily imply better visibility for the features of interest. Sufficient relative contrast among features is needed to see these features in an image.

Comparison of light–tissue interactions for visible and near infrared wavelengths using a SLO

To obtain useful images with infrared illumination, which is absorbed to a lesser degree than visible light, it is necessary to control the light that scatters multiple times over a wide region of the fundus. The optics of the SLO provide several ways to improve contrast over fundus camera imaging (Webb et al., 1987). First, the SLO illuminates only a small region of the fundus at a time, quite different from the fundus camera which illuminates the entire field of view. Second, the SLO captures the light returning at the time of illumination, so that only light returning to the detector from the illuminated point is assigned to that point in the image. Third, a selection of apertures conjugate to the retinal plane permits the spatial sampling of the light returning from the fundus (Elsner et al., 1990, 1992a).

Mode of imaging

The mode of imaging is determined by the selection of aperture in a confocal imaging system (Webb et al., 1987; Elsner et al., 1990, 1992a; Elsner, Burns & Weiter, 1992b) [Fig. 2(B and C)]. In direct mode imaging, the smaller the aperture, the more the image is determined from directly reflecting or backscattered light from the plane of focus (Webb & Delori, 1988; Elsner et al., 1990, 1992a, b). In indirect mode imaging, reflections on the axis of the optical path are blocked by an annular stop; light that is more laterally scattered or scattered from more distant planes is included in the sampled light (Elsner et al., 1992a, b, 1993). The appearance and the contrast of retinal features change with both wavelength (488–790 nm) and diameter of apertures (Webb & Delori, 1988; Elsner et al., 1990). We investigated indirect mode imaging and a wider wavelength range in the near infrared, with the emphasis on sub-retinal structures.

METHOD

Subjects

Fifty normal subjects of a wide range of age (Table 1) and ocular pigmentation were studied to determine when the beginning of sub-retinal pathology could be detected, as well as the generality of appearance of fundus features in infrared light. To quantify the effects of wavelength and imaging mode, 16 of these subjects were tested with

TABLE 1. Age in years of normal subjects tested with near infrared light

Age in years	Male	Female	Total
0–12	10	2	12
20–30	8	5	13
30–40	6	3	9
40–50	5	4	9
50–60	4	0	4
60–70	1	1	2
70–80	1	0	1

mydriatic pupils, using at least one visible and one infrared wavelength per subject.

To examine the effects of wavelength and imaging mode on the contrast of features, and to quantify the number of sub-retinal features seen clinically as opposed to in monochromatic light with an SLO, 6 subjects were tested. These subjects were without ocular complaint other than refractive error (26–54 yr, 3 males and 3 females). Their pupils were dilated, then each subject was carefully examined by a retinal specialist with indirect ophthalmoscopy and slit lamp biomicroscopy to identify the location and number of drusen, as well as to ascertain normal retinal status. The five Caucasians and one Oriental have a full range of eye color: blue (2), hazel (1), and brown–dark brown (3).

Patients

To investigate the appearance and contrast of features in diseased eyes for visible as opposed to infrared light, patients with retinal and choroidal disease, ages 3–95 yr have been tested, to date more than 100. Pigmentation ranged from albino to darkly pigmented fundi. To investigate the effects of a series of near infrared wavelengths on the contrast of subtle changes, 5 patients with early (non-exudative, lack of widespread atrophy) AMD were recruited. To investigate the effects of a series of near infrared wavelengths on the contrast of features associated with a high risk of vision loss, 20 additional patients with exudative AMD were recruited (with preliminary results presented in Elsner, Staurenghi, Weiter, Buzney, Wolf & Wald, 1993). Sample results are shown for 1 patient with early AMD and 1 with exudative changes.

Patients typically are dilated, then examined by a retinal specialist with indirect ophthalmoscopy and slit lamp biomicroscopy prior to study. The research followed the tenets of the Helsinki agreement, informed consent was obtained from all subjects and patients in this communication after the nature and possible consequences of the study were explained, and the research was approved by the Schepens Eye Research Institutional Review Board for Human Subjects.

Procedure

We made all measurements with a research SLO designed for quantitative reflectometry (Elsner *et al.*, 1990, 1992a), which has a silicon solid state detector that retains sensitivity throughout the near infrared spectral region. A sixth laser system (Ti:Sapphire, Titan CW, SEO, pumped by an Argon laser from American Laser) was added to investigate the effects of infrared wavelength, including 795–895 nm. This provided a single, tunable, solid state laser source that was monochromatic (<1 nm at half-height), was well-collimated along all radii, had a narrow Gaussian beam prior to entering the instrument (2.1 mm at $1/e^2$), and had constant polarization across wavelength. All laser beams are combined prior to entering a 1 mm entry port to the scanning system.

The primary aperture was 4 mm in diameter; it is conjugate to the retinal plane and corresponds to 400 or 800 μm on the retina for the large (29 × 23 deg) and small (15 × 13 deg) field sizes, respectively. This aperture eliminates corneal reflection and provides a good image. Additional apertures included confocal apertures with outer diameters of 1 mm (100 or 200 μm at the retina) or 2 mm (200 or 400 μm) or indirect mode apertures with stops of 1 (100 or 200 μm) or 4 mm (400 or 800 μm) with an outer diameter of 2.3 mm (2300 μm or 4600 μm). More light is required to preserve image quality for a 1 mm aperture or 4 mm stop. The free area of the aperture with respect to the retina for the small field size is about 1.3×10^5 vs $4.5 \times 10^6 \mu m^2$ for the primary aperture and its converse (400 μm stop), respectively.

Laser wavelengths (488, 514, 543, 594, 633, and 805–895 nm) were calibrated for power (EG&G 2550) at the cornea. For quantitative comparisons for visible vs infrared wavelengths, laser power was held constant for all imaging modes at a given wavelength, set to the power required to bring the primary aperture image into a fixed range of gray scale values. Laser power was typically less than 50 μW per 0.2 or 0.6 cm^2 (<250 μW/cm^2) on the retina at the primary aperture for any wavelength tested. The near infrared power was typically 67 μW/cm^2 with the large field size. For the quantitative comparison of contrast for a series of near infrared wavelengths, wavelength was tuned under computer control, then power was adjusted with a neutral density wedge to keep image gray scale constant, which required only a few seconds. The video gain of the detector was recorded and calibrated across wavelength. The detection system was linear, but video gain was held constant.

Unless otherwise indicated, data were from fovea-centered images. The plane of focus was adjusted for each wavelength so that the sides of retinal arterioles and venules were in sharpest focus, regardless of the appearance of smaller vessels or other features. Target vessels for the large field were at the arcades and for the small field at the macular arterioles and venules. Quantitative reflectance data were collected as 8-bit 512 × 480 pixel (Imaging Technology FG100 AT) images. Sessions were also documented on S-VHS videotape (60 Hz field rate). Taping allows the documentation of relative depth and thickness, during focusing or eye movements. Data acquisition from tape was used when either areas of the fundus are not digitized during the session or comparison of fundus features to visual stimuli was needed (8 bit, 640 × 480 pixels, Data Translation 2867, Global Lab Image).

Data analysis

Digital image processing is used to obtain quantitative measures. For noise reduction, two to four images are averaged. Regions of interest for quantification are selected based on (1) the presence of a given feature across all conditions, (2) the absence of artifact in the region of interest, and (3) the presence
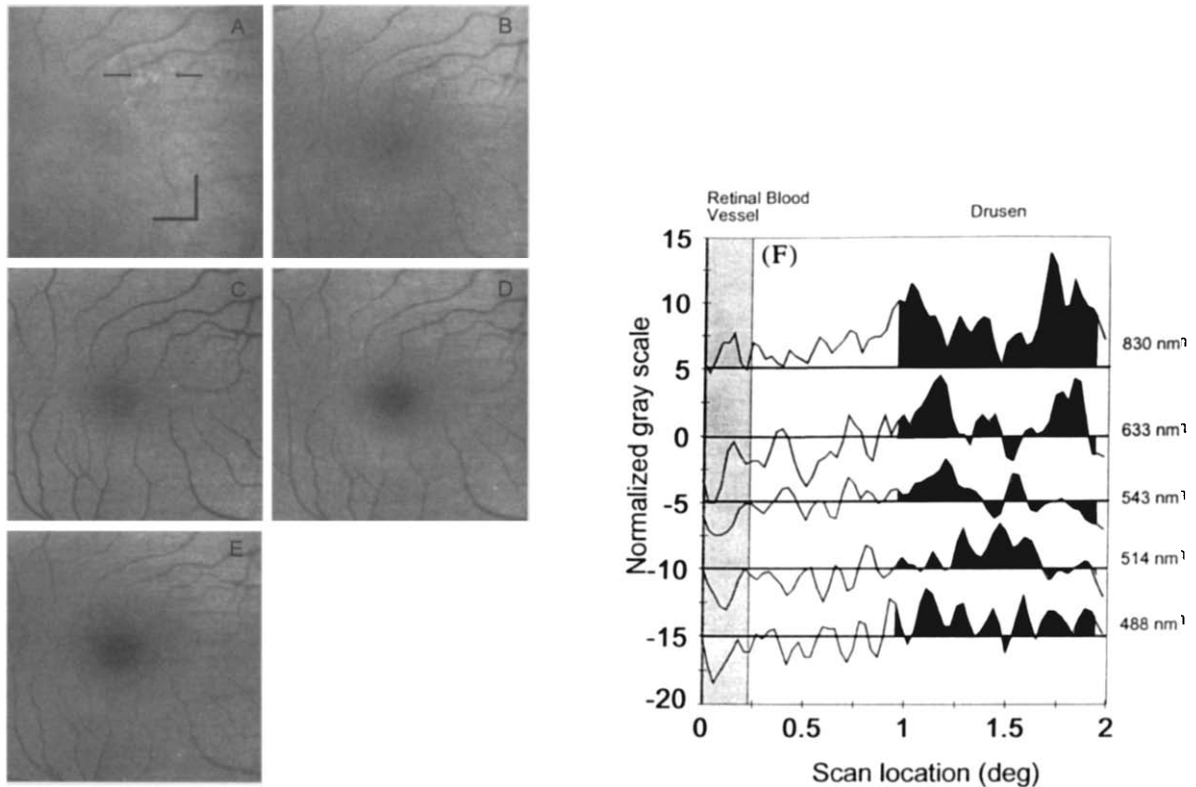
FIGURE 3. The effects of wavelength in visualizing sub-retinal structures in a clinically normal subject with light fundus pigmentation (41 yr). Direct mode image (400 μm aperture) at small field size. Only the central portion of each image is displayed. The size calibration is shown, with the orthogonal horizontal and vertical bars in (A) each representing 2 deg. The region collinear with the two horizontal lines is the drusen test area for the gray scale computations. The test area begins with the retinal vessel crossed by the left line and ends 2 deg to the right, after the whitish area. (A) 830 nm, (B) 633 nm, (C) 543 nm, (D) 514 nm and (E) 488 nm. (F) Normalized gray scale values for a 70 pixel horizontal scan over the drusen, computed as a z-score (the gray scale value minus the mean of a reference area, divided by the standard deviation of the reference). Higher values indicate brighter fundus values. Curves have been slid vertically to eliminate overlap, with the mean value for each wavelength represented by the horizontal lines.

of accurate landmarks in all images. Clearly, some comparisons cannot be made between direct and indirect images, since the same landmarks are not visible. To quantify a region of interest or a reference region, the mean and standard deviation of the gray level is calculated for a 10 × 10 pixel area; coefficient of variation of gray level is calculated as the standard deviation divided by the mean. In addition, we computed the normalized gray level across a horizontal scan (Fig. 3). Normalized values (z-scores, 99 df) are computed by subtracting the mean of a reference area, then dividing this difference by the standard deviation of the reference area.

RESULTS

The contrast of fundus features varies both with wavelength and imaging mode. In the direct mode, good contrast images were obtained at all wavelengths, including infrared wavelengths not previously used for imaging. The visibility of features depended on wavelength, particularly in indirect mode (see below). The light levels needed to acquire infrared images were comfortable, even to children, and invisible to most patients.

Quantitative comparisons of infrared vs visible wavelengths

For the primary aperture, the foveal region appears lighter with increasing wavelength, consistent with decreased absorption by macular and other pigments (Figs 3–5). At wavelengths from 488–633 nm, the presence of unbleached photopigment darkens the fundus, particularly for wavelengths near the maximum absorption for cone photopigment, 543 and 594 nm. A uniform appearance across the fovea is obtained following exposure to bleaching lights for 594 nm light and longer, but not with shorter wavelengths (Fig. 3).

Clinical examination in the 6 subjects selected for quantitative study revealed only 2–3 small Drusen (<75 μm) in 3 of 6 subjects. Yet 5 of 6 had several sub-retinal structures seen with 830 nm light and the primary aperture (Figs 3–5), with some structures exceeding 500 μm in diameter. These were not visible to the same extent at 633 nm, and less visible with 543 nm, which revealed only the 2–3 small drusen and other features seen clinically. Of the 3 subjects without clinical findings, 2 subjects (including the oldest subject) had sub-retinal, placoid patches with indistinct borders in infrared imaging. All these findings were far more subtle, i.e. smaller or of lower contrast, than those seen

in patients with AMD. The other subject had no detectable pathology within the macula with any method used.

The greater visibility of the drusen is accounted for by two factors. First, the region containing drusen (Fig. 3) is significantly brighter for the longer wavelengths, with respect to a reference area (z-score = 7.36 for 830 nm and 10.5 for 633 nm). This region is no different or darker for shorter wavelengths (z-score = 0.088, −4.493, and −1.893) for 543, 514, and 488 nm, respectively. Second, the lowest standard deviation of gray scale over uniform sub-retinal structure is for the 830 nm condition. The larger variation in gray scale typically found for other wavelengths is attributed to other retinal features, e.g. nerve fiber layer or small retinal vessels.

Comparisons of direct vs indirect aperture

The change in the amount of light returning from the fundus for direct vs indirect modes as a function of wavelength is shown in Fig. 4. When the 6 normal subjects, who were examined also with wavelengths 488, 514, 543, and 594 nm, and with both direct and indirect modes, shorter wavelengths showed less or the same amount of detail of sub-retinal features (Figs 3–5).

The relative amount of light returned for indirect vs. direct mode increases with increasing wavelength [Fig. 4(B, D and E)]. For 543 nm, the macula in indirect mode is much darker than in direct mode [Fig. 4(E vs F)]. For 830 nm, there is little difference, and sometimes more light is returned in indirect mode [Fig. 4(A vs B)]. For many subjects indirect mode images at wavelengths less than 543 nm were too dim to provide data and are not included in summary data analysis, which shows the ratio of two indirect mode apertures to the primary aperture [Fig. 4(G)]. The exception is an Oriental subject with a tigroid fundus (triangles).

The spatial distribution of light returning from the fundus changed with wavelength, and was more widely
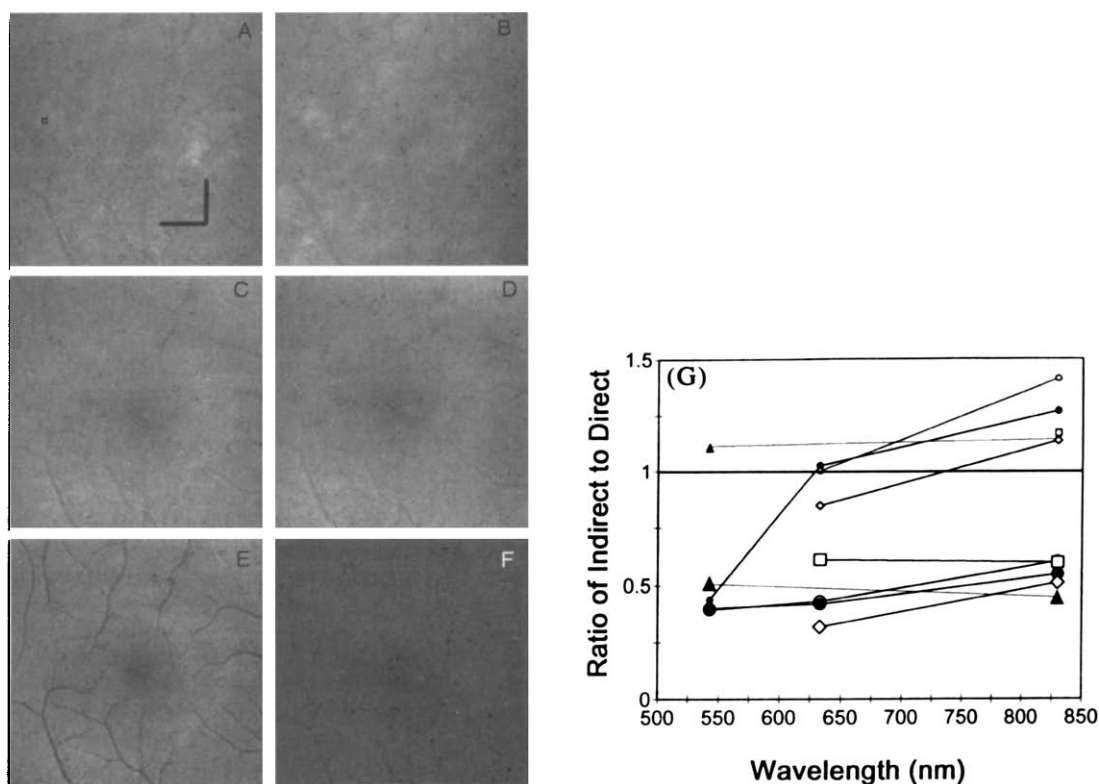

FIGURE 4. The effects of wavelength (rows) and imaging mode (left vs right columns) in visualizing sub-retinal structures in a clinically normal subject (29 yr) with moderate ocular pigmentation. All panels show the central portion of small field images, with the orthogonal horizontal and vertical bars in (A) each representing 2 deg. For a given wavelength, the illumination is constant for all imaging modes, so that the change in the amount of light returning from the fundus can be measured directly. (A) 830 nm, direct mode (400 μm aperture), showing bright sub-retinal structures covering the entire image. The box provides the mean and standard deviation for the quantitative comparisons in the text and in G. (B) 830 nm, indirect mode (200 μm stop), showing sub-retinal structures well, but not as bright as in (A). Little more was revealed by a larger stop, indicating these structures have little thickness. (C) 633 nm, direct mode (400 μm aperture), showing some bright sub-retinal structures covering the entire image. (D) 633 nm, small field, indirect mode (200 μw stop), showing fewer sub-retinal structures, but more retinal detail than (B). (E) 543 nm, direct mode (400 μm aperture), showing the fewest bright structures of all direct mode images. The fovea is darker than more peripheral retina, and this obscures the view of the sub-retinal structures. There is excellent visibility of the retinal vessels overlying sub-retinal structures. (F) 543 nm, small field, indirect mode (200 μw stop, revealing little but the foveal reflex, since little light is returned from the fundus. The larger stop produced an image too dim to quantify. (G) Ratio of light returning from the fundus for indirect vs direct (400 μm aperture) imaging. Small symbols, 100 μm stop; large symbols, 400 μm stop. Open symbols, subjects with lightly or moderately pigmented fundi. Closed symbols, subjects with darkly pigmented fundi.

spread for the longer wavelengths. At 830 nm, more light is returned through the indirect aperture with the 100 μm stop, than through the direct aperture with the 400 μm aperture [Fig. 4(G)]. At 633 nm, the two apertures pass a similar amount of light. At 543 nm and shorter wavelengths, much less light is typically returned with this indirect aperture.

There is a sharp decline in the amount of light collected from the fundus for the large stops [Fig. 4(G), 400 μm, large symbols] vs the small stops (100 μm, small symbols). Even with 830 nm light there is only about 50% as much light returning through a 400 μm stop as through a 400 μm aperture, despite having a free area of the aperture more than ten times greater. The amount of light returning is similar for smaller indirect (100 μm aperture) and direct modes, although the aperture free area is about 38 times greater. This indicates that the measurements of the lateral spread of light on the fundus, as well as the quality of the image, are less influenced by the most peripheral portions of the apertures than by the more central portions.

Contrast in the near infrared

Six patients with early (dry) AMD were selected for comparison of the contrast of sub-retinal features in a series of near infrared wavelengths. Generally, wavelengths of 820 nm or longer provided a clearer image of sub-retinal structures than shorter wavelengths, for which apparent contrast was poorer [see Fig. 6(A)]. Specifically, the contrast of a sub-retinal blood vessel in direct mode, measured as the coefficient of variation, increases with increasing wavelength [Fig. 6(B)]. The apparent contrast was in general agreement, since the blood vessel was invisible at wavelengths shorter than indicated by the vertical bar (on the computer monitor at any contrast setting), but is quite visible at all the longer wavelengths tested. The standard deviation increased [Fig. 6(B)] in a similar manner, indicating that the procedure to maintain constant gray scale succeeded.

Fundus appearance with imaging mode

The qualitative conclusions concerning fundus appearance and direction of contrast (positive or negative) in visible through near infrared wavelengths are summarized in Table 2, which combines data from all normal subjects and patients in Experiment 2. The near infrared wavelengths are roughly divided into two wavelength regions (780–820 and 825–895 nm), since the most noticeable improvement in visualizing sub-retinal features occurs between these two regions (see below). Changes within these regions are subtler, depending on fundus pigmentation, pathology, and media.

Direct mode images had good contrast for retinal vessels and other superficial structures at all illumination wavelengths tested. The retinal features including the nerve fiber layer are seen for the smallest aperture at all wavelengths, if this layer is in focus, e.g. the papillomacular bundle [Fig. 5(E)]. While the plane of focus of

the instrument and the optics of the eye are potential factors in the difference between Fig. 5(A vs E), our plane of focus is relatively thick. Manipulating the plane of focus or imaging mode could not produce images for the young subject that had sub-retinal structures similar to the older subject. Conversely, manipulating the plane of focus in older adults can produce an excellent image of the nerve fiber layer, but it is typically less bright and of lower contrast. Aging factors must be further studied, e.g. changes in the thickness and composition of absorbing and scattering layers.

As aperture size increased in the direct mode, the superficial layers appeared lower in contrast, particularly for wavelengths of ≥633 nm. The deeper structures, e.g. choroidal blood vessels and choroidal pigment were more visible with larger apertures, but typically only for longer wavelengths.

In indirect mode imaging, fewer details of retinal features are seen. The contrast of retinal features is particularly degraded in indirect mode with infrared light, as seen in the direct vs indirect image comparison in Figs 4(A vs B), 5(A vs C and D). The contrast degradation for retinal features is shown for shorter wavelengths in Fig. 4(C vs D and E vs F).

Fundus features

Choroidal vessels are seen readily in the normal eye with near infrared [Fig. 5(C, D and F)] imaging and less well with other wavelengths (Figs 3–4). The choroidal vessel contrast for infrared is usually negative (dark vessels on light fundus background) for all imaging modes (noted as "--" or "-" in Table 2). Retinal vessels appear dark or have dark borders for all wavelengths in direct mode imaging [infrared images in Figs 3(A), 4(A), 5(A, E and F), 6(A), and 7(E, G and H), visible wavelength images in Figs 3(B–F), 4(C and E), and 5(B)].

The optic disk rim appears dark with respect to the surrounding fundus at all wavelengths in confocal mode. However, in indirect mode, the optic disk rim appears dark at wavelengths longer than about 820 nm, in contrast to the light appearance for wavelengths of 790 nm and less. The optic disk in pathological eyes can appear pale, especially in patients with dark pigmentation or pathology near the disk, such as a retinal detachment or staphlyoma. The lamina cribrosa appears light and is often well-visualized in older patients.

Imaging of pathological features in direct mode

With near infrared imaging (wavelengths ≥ about 820 nm) retinal and sub-retinal structures are well-visualized despite the presence of cataract or hemorrhage (Fig. 7). Sub-retinal pathology is seen to a much greater extent with infrared imaging than with routine clinical techniques (Figs 5–7).

Sub-retinal deposits near the plane of focus appear light in direct mode, partially blocking the view of choroidal vessels (Figs 3–7). These deposits are never seen in subjects under the age of 20 yr and are usually small (<25 μm in diameter) in subjects 20–50 yr. These
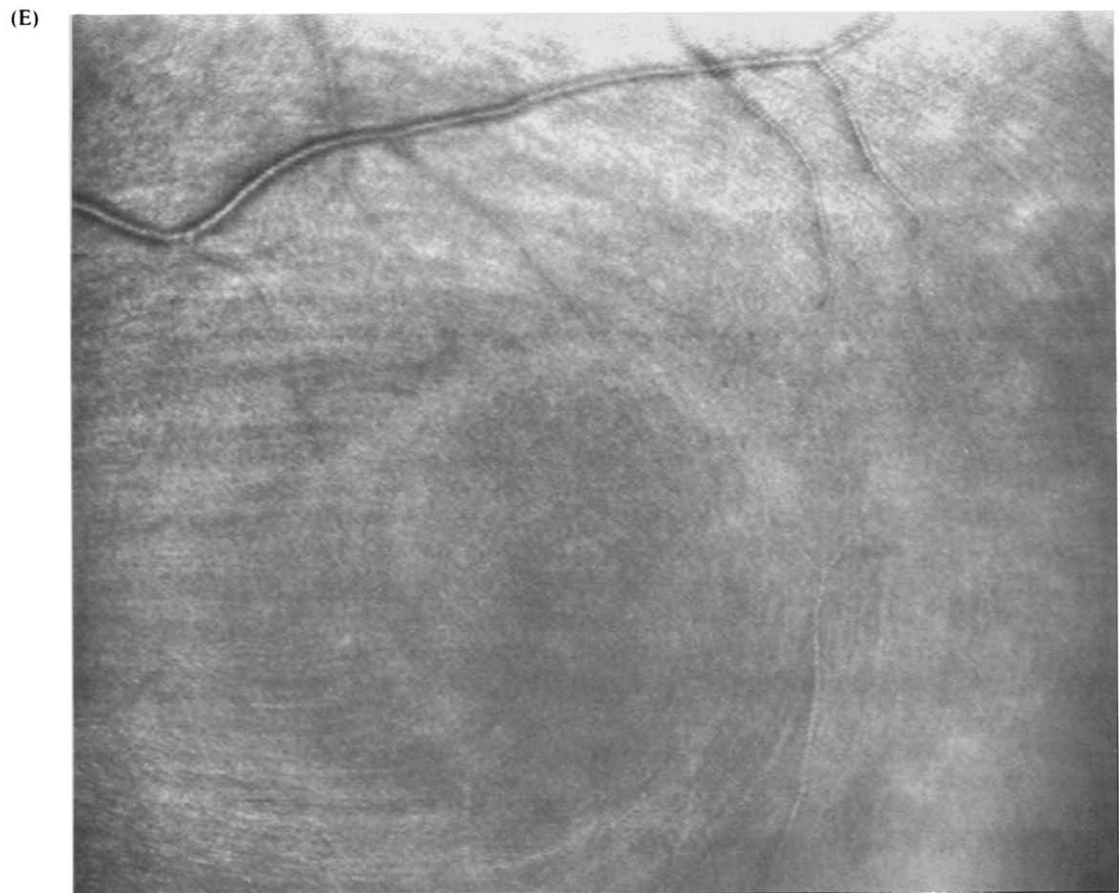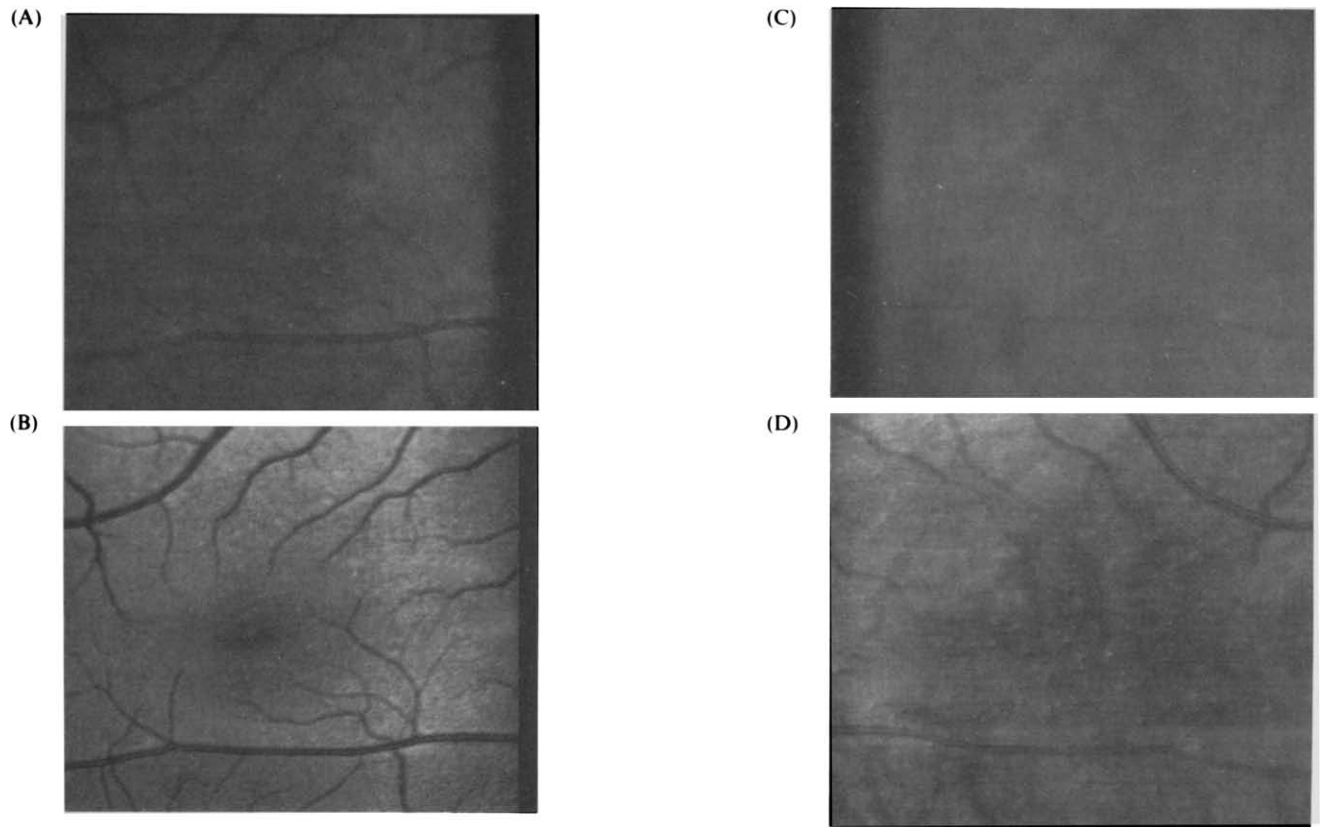
(A)

(C)

(B)

(D)

(E)

FIGURE 5 (A–E). Caption on facing page.

(F)

FIGURE 5. The appearance of retinal and sub-retinal features in young eyes without pathology, showing interaction of the effects of wavelength and imaging mode. (A) Small field, foveal centered view in direct mode (400 μm aperture) at 830 nm. Sub-retinal structures are seen as light areas in a subject with moderate ocular pigmentation (40 yr). (B) Same, but with 543 nm. Retinal vessels are seen better at these wavelengths, but the view of underlying features is poor (shown in Elsner et al., 1993). (C) Same view, indirect mode (400 μm stop) image at 830 nm (shown in Elsner et al., 1993). Sub-retinal features are noticeably thickened, especially when viewed at video rates. (D) Same view, indirect mode (400 μm stop) image at 835 nm. Image contrast is improved by increasing the light level and using the Ti:sapphire laser. Sub-retinal features appear rock-like. (E) The 5-yr-old daughter of this subject, without mydriatics but in a dimly illuminated room, at 830 nm and in direct mode (400 μm aperture). (F) A disk-centered view of a 44-yr-old male, large field size, direct mode (400 μm aperture), showing the nerve head rim and blood vessels as dark. The focus is slightly deeper than the previous view, which de-emphasizes the nerve fiber layer, especially in subjects beyond their third decade.

are always seen in patients with AMD, except when examining areas of atrophy, scars, or dense hemorrhage and correspond to drusen as seen with fluorescein angiography. Sub-retinal deposits are readily seen in undilated subjects, with older observers sometimes showing large placoid structures that partially obscure the choroidal vessels beneath them.

In the patients with exudative AMD and pigment epithelial detachment, drusen were well-seen [e.g. Fig. 7(E, G and H). The drusen seen in infrared light were not seen to the same extent at 594 nm. There are two key advantages to this method of imaging that are not represented by photographic prints due to non-linear gray scales or limited dynamic range. First, the drusen surrounding the detached region appear similar to those lying above the detachment [Fig. 7(E, G and H)], although the difference in the gray scales of the background obscures this finding. Second, retinal and sub-retinal features such as drusen are seen even over regions of sub-retinal hemorrhage (darkened region). Several regions have extensive choroidal depigmentation changes [Fig. 7(B)], and thus it is not possible in one

image to represent such very bright areas and also the dimmer region in the area of the detachment. Focusing did not provide further information about the layers within or beneath the layers of the pigment epithelial detachment, indicating little light returned.

Scars, such as those following resolution of choroidal new vessesls or laser photocoagulation, appear bright. Scars, atrophic regions, and some types of deposits are so highly reflective that to obtain an image of these, the light level must be reduced beyond that useful for the surrounding fundus. It is common for a scar to return more than 100 times more light than the surrounding fundus.

Pathological features in indirect mode

Bright features block light from reaching the structures beneath them, so these deeper layers must be imaged differently, such as with indirect mode, which can provide an image similar to side or retro-illumination. Topographical changes are particularly emphasized in the deeper layers, such as thickness changes due to areas of atrophy, fluid accumulation, or
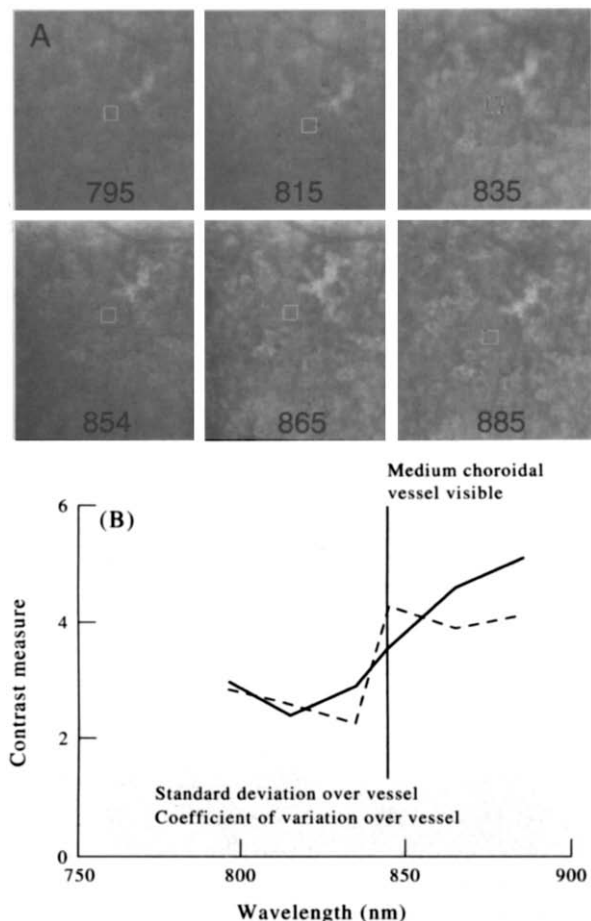
FIGURE 6. A Comparison of a choroidal vessel as a function of wavelength in the near infrared region. Images are of a patient with early AMD, taken at the small field size in direct mode (400 μm aperture). The area within the square is the test region for computation of the contrast of the choroidal vessel. (B) Contrast for the test, computed as the coefficient of variation. The vertical line indicates the wavelength region above which this vessel became visible for this eye. The standard deviation for the test region, also shown, is in good agreement; this indicates that the manipulation to maintain constant gray level was successful.

choroidal new vessels (Fig. 7), or sub-retinal deposits (Figs 3–6). These can be seen only when there is either sufficient thickness or differences in refractive indices sufficient to change the light path, as well as sufficient light reaching the structures and returning through the more anterior layers. While tissue beneath sub-retinal hemorrhages often can be visualized by increasing light level, large scars or large areas of turbid fluid make it difficult to visualize potential pathology underlying them with indirect, as well as direct, mode.

DISCUSSION

The clinical hallmark of the non-exudative form of AMD is drusen. Number, location, type, and size have been considerations (Bressler, Bressler, Seddon, Gragoudas & Jacobsen, 1988; Eisner, Stoumbos, Klein & Fleming, 1991). Determining who is at risk for visual loss due to AMD is difficult for several reasons. First, with clinical examination or fundus photography, drusen are often obscured by media changes in an aging

population. Small drusen are not resolved, and contrast is reduced for the borders of soft drusen. This influences the classification of "hard vs soft' drusen and "large vs small" drusen. For quantitative studies, only a fraction of potential patients can be evaluated (Sebag, Peli & Lahav, 1991). Second, there are large individual differences in fundus appearance and drusen visibility due to the variation in the concentration of ocular pigments, such as melanin, across individuals (Delori *et al.*, 1977; Weiter, Delori, Wing & Fitch, 1986) and over time (Boulton *et al.*, 1990). The pattern and number of drusen seen in photographs changes over time, not always monotonically (Sebag *et al.*, 1991). Most significantly, features identified in photography as drusen have been found to be atrophic regions on examination with histology (Bressler *et al.*, 1994). Consistent with these findings, in Fig. 5(A and B) at the vessel branch at about 5 o'clock with respect to the fovea can be seen an example of a window defect (depigmented spot) which could be mistaken for a druse. This region has no increased thickness when seen in indirect mode [Fig. 5(C and D)]. Conversely, in both normal adults and patients, we found many thickened structures that were undetectable in visible wavelength light.

To improve imaging of sub-retinal structures, we used infrared light, which passed readily into and out of the deeper fundus layers, with little visual consequence or pupil constriction (Wyszecki & Stiles, 1982b). In the past, infrared photography for this purpose produced images of low quality, used primarily for large, pigmented structures such as choroidal melanoma (Bonin *et al.*, 1990). A coarse film grain and the difficulty in interpretation of color images left the clinical usefulness in question (Jaeger, Gotz & Blankenagel, 1986). The impetus for continued research arose from (1) fluorescence angiography (Flower & Hochheimer, 1973; Destro & Puliafito, 1989), e.g. indocyanine green angiography, with an excitation peak at 805 nm; (2) infrared photocoagulation techniques, with and without infrared absorbing dyes, and the absorption in the pigment epithelium and choroid (Gabel *et al.*, 1978), and (3) fundus imaging during functional assessment of the retina, eye movements, focusing a non-mydriatic camera, or pediatric uses (e.g. Fausset & Enoch, 1987; Sunness, Johnson, Massof & Marcus, 1988). The chief advantages of infrared imaging were the comfortable light levels and pupil dilation without mydriatics.

Resolution and contrast

The spatial resolution and the contrast of images illuminated in the near infrared, in the past was reduced by poor optical throughput and blur, resulting in dim or low contrast images. The design of instruments using infrared light was often made far more complex than that used successfully with a model eye or visible light; for instance, with 900 nm *in vivo* the principle reflector in the fundus differed systematically from that in visible light, and the width of the point spread function on the eye was more than 20 times that for visible light (Cornsweet & Crane, 1970). Modern instruments (e.g.

Destro & Puliafito, 1989) have improved technology: optical coatings that efficiently reflect infrared light, plus digital presentation or storage. Video systems permit the real-time variation in the depth of focus or z-axis to be visualized. Only if the operator focuses on the fundus in infrared light will there be little blur from the several diopters of chromatic aberration of the eye (Wyszecki & Stiles, 1982a).

Limits on image quality remain, due to lack of resolution of the optics of the eye; poor light return from the eye; and the limited dynamic range of the detector, the video standard, and digitizing systems. Consider the resolution required to resolve two adjacent structures (which is different from detecting a high contrast structure on a background). The minimum resolvable lateral spacing with normal illumination by coherent radiation (d_{min}) is given by:

$$d_{min} = \lambda/n \times \sin(\alpha) \tag{1}$$

where λ is the wavelength, n is the index of refraction, and α is the aperture angle of the lens (Slayter & Slayter, 1992). The denominator is known as numerical aperture (NA). Clearly, the lateral resolution decreases with increasing wavelength. For the human eye *in vivo*, the maximum acuity is obtained with a 2.5 mm pupil and a larger pupil results in optical degradation (Campbell & Gubisch, 1966). Thus, the NA aperture of the eye is about 0.08, which gives a resolution limit of 4.25 vs 6.3 μm for 550 vs 830 nm, respectively. For an image with a field of view that extends 15 deg, the best theoretical resolution of a human eye for 830 nm light is limited to about 700 picture elements (pixels), or 350 pairs of elements.

Poor return of light limits image quality for *in vivo*, confocal imaging systems; the size of the pinhole must be large enough to overcome the lack of light returning through the pupil of the eye. This relatively large confocal aperture and small NA limit the axial resolution (e.g. about 240 μm for 830 nm), although inter-polation between confocal sections will allow discrimination in depth of 35 μm (Bartsch & Freeman, 1994). While there is a loss of resolution due to increasing the wavelength, this loss is relatively less important than increasing NA, so long as there is sufficient light returning to the detector.

In near infrared illumination, blood components, including hemoglobin and oxygenated hemoglobin as well as water, are the most important potential absorbing pigments in the normal fundus; thus large, perfused vessels appear dark *in vivo*. A less obvious effect is that at shorter wavelengths, there is an absorption of multiply scattered light; at near infrared wavelengths, the ocular globe is more similar to an integrating sphere. This provides trans- and retro-illumination by infrared light of features in deeper layers. When blood content is decreased, the effects of absorption are noticeably missing. Thus, in atrophic or ischemic tissues it might be possible to obtain long range scattering in short wavelength illumination, as well as in infrared illumination.

Contrast is affected not only by optical factors, but also by sampling artifact in the imaging acquisition system. Digitization errors can occur when sampling with only 8 bits, which provides a scale too insensitive for some conditions (Elsner *et al.*, 1992a) so that subtle detail is lost. Another problem occurs when the dynamic range needed to represent both bright and dark structures accurately exceeds the dynamic range of the digitizing system (Fig. 7), especially with scars. There are too few steps available over too great an intensity range in the pathological fundus. Either the dark part of the image is too dim to include useful contrast or the bright part of the image is saturated. In extreme cases, the detector or video specifications are exceeded by the light returned by a scar or atrophic tissues. In many digital systems, but not photographic systems, the images are viewed nearly continuously during acquisition, and the

TABLE 2. Visibility of fundus features in different wavelengths and imaging modes

Fundus features	Mode of imaging	488, 514, 543 nm	594 nm	633 nm	780–820 nm	825–895 nm
Retinal vessels	direct	− −	− −	− −	− −	− −
	indirect	*	−	+	+	+/−
Nerve fiber layer†	direct	+ +	+	+	+	+
	indirect	*	0	0	0	0
Optic disk rim	direct	− −	− −	− −	− −	− −
	indirect	*	+ +	+ +	−	−
Choroidal vessels	direct	0/+	0/+	+	− −	− −
	indirect‡	*	0/+	+/−	−	−
Sub-retinal deposits	direct	§+	+	+	+	+ +
	indirect	*	0/+	+	¶+/−	¶+/−
Sub-retinal hemorrhage	direct	− −	− −	−	0/−	0/−
hemorrhage	indirect	*	− −	?	0/−	0/−

*At these wavelengths indirect mode requires higher light levels than used in this study to obtain useful images.
†Papillo-macular bundle best visilble at 633 nm, optic disk head region best visible at 488 nm.
‡Contrast varies greatly with fundus pigmentation, different vessels emphasized.
§Not well seen in darkly pigmented regions, i.e. under macular pigment.
¶Thickened structures appear to cast a shadow.
+ +, much lighter than surrounding fundus (positive contrast); + lighter than surrounding fundus; 0, not visible; −, darker than surrounding fundus; − −, much darker than surrounding fundus; 0/−, darker if seen; 0/+, lighter if seen; +/0, light or dark.
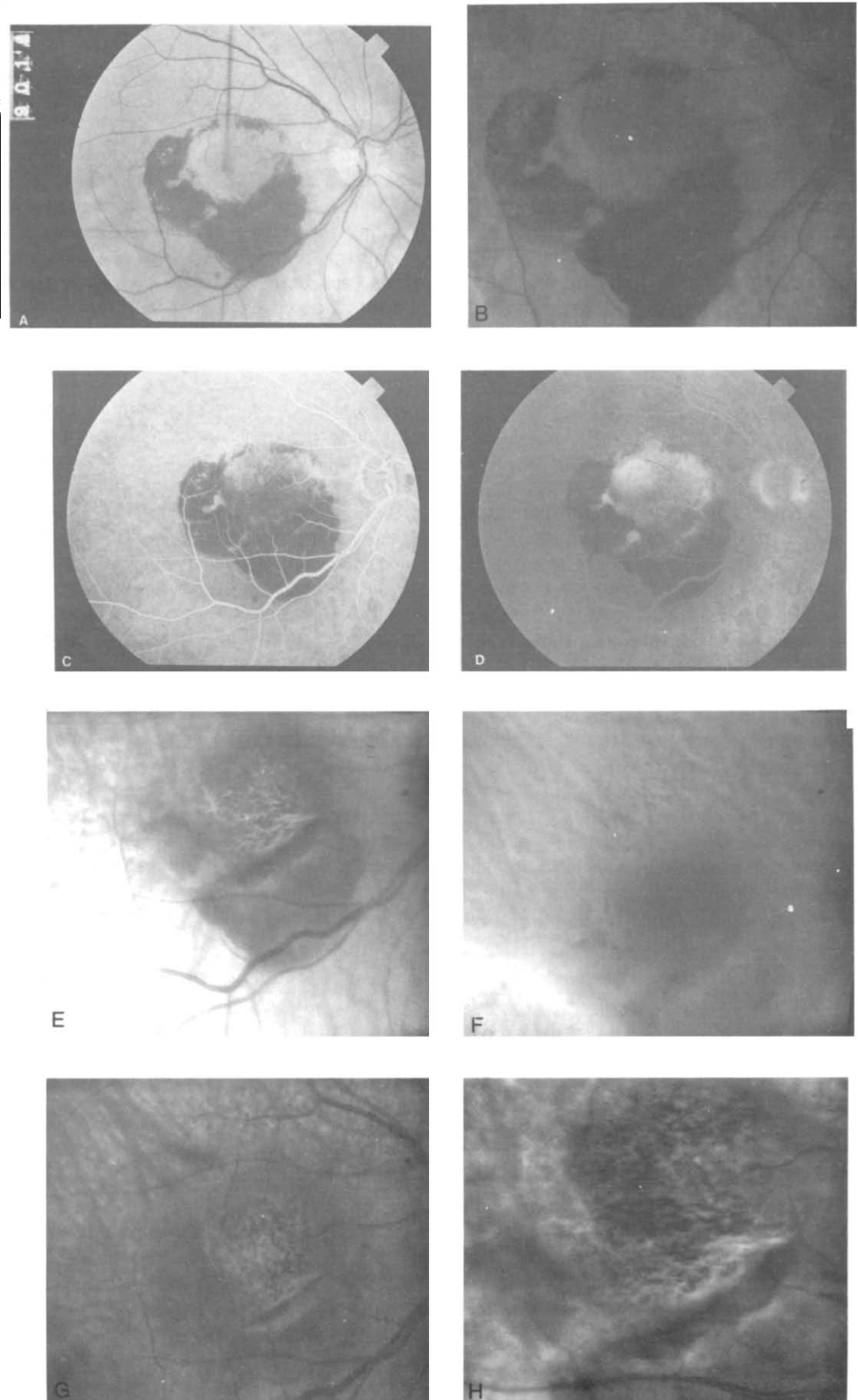
FIGURE 7. Ca   n on facing page.

wavelength, light level, plane of focus, or aperture is readily maximized.

Separation of reflected and multiply scattered light

Using infrared light and an SLO provides benefits from both the greater return of light from the deeper layers and the discrimination of reflected or back-scattered light from multiply scattered light. Previous studies with monochromatic photography (Delori et al., 1977; Ducrey et al., 1979), reflectometry (van Norren & Tiemeijer, 1986; Delori & Pflibsen, 1989), and SLO imaging (Webb & Delori, 1988; Elsner et al., 1990) have shown the benefits of separating information from different fundus tissues by manipulating the illumination wavelength. The wavelength of the illumination light particularly influences the information carried in the light returning from the deeper fundus tissues. Long wavelength light passes more readily into the deeper layers of the fundus and returns, carrying information concerning the relative contrasts of the major absorbers. Some of this light has been reflected or backscattered, but some has been multiply scattered from structures at some distance superficial to, deeper than, or lateral to the feature of interest. Imaging systems that cannot separate this scattered light, such as a commercial fundus camera, provide images that include both the scattered light and the reflected light, decreasing the contrast for either type of information, particularly at longer wavelengths. This leads to high contrast images of superficial features only at short wavelengths ($\lambda < 600$ nm), as well as an overall reduction of contrast of middle to longer wavelengths ($\lambda > 600$ nm). Thus, retinal vessels become invisible in long wavelength light, especially in the case of arteries, while these are seen quite well at similar wavelengths with an SLO (Elsner et al., 1990). High contrast views

of deeper layers are difficult to obtain in a normally pigmented fundus without an SLO. With an SLO, the change in the image with wavelength is least apparent with the smallest confocal aperture, as previously found (Webb & Delori, 1988; Elsner et al., 1990). The appearance of the fundus with an SLO at 594 nm for both bleached and unbleached retinas, and direct and indirect modes, has been described in detail, since it is used for cone retinal densitometry (Elsner et al., 1992a, b).

The light returning from the ocular media or deeper layers, which would reduce the contrast of features from the layer of interest, must be carefully controlled. This unwanted light is scattered outside a small detection aperture (the confocal mode of imaging with the SLO), partially enters a larger detection aperture (the open mode of the SLO), and can reach the film from many points on the fundus to a large extent at long wavelengths (fundus photography). If the information from the deeper layers or from lateral scattering is needed, without reduction in contrast by the directly returning light, then the directly returning light is blocked (indirect mode).

Sub-retinal features and clinical implications

Improved contrast with infrared imaging, despite a potential loss of spatial resolution, is the likely reason for better detection of both small and large sub-retinal structures, although observations of the features detected are in agreement with the theoretical size limitations. Confocal imaging emphasizes thin or highly reflective features, such as calcified drusen, and allowed visualization of pathology near scattering bodies, such as scars. Indirect mode imaging emphasized structures that were thick, scattered light laterally, or were visualized by side illumination or retro-illumination, such as

FIGURE 7 (opposite). Comparison of images in an AMD patient (78 yr) with a cataract, a hemorrhagic pigment epithelial detachment (PED), and drusen. (A) A red-free fundus photograph of a patient showing a PED (circular area surrounding fixation target), surrounded by hemorrhage. The layers in the vicinity of the blood are poorly visualized. The fundus region over the detachment and the drusen are not well visualized. (B) 594 nm SLO image, large field, indirect mode (200 μm stop), which shows clearly the sub-retinal hemorrhage, but little detail of sub-retinal pathology. Choroidal vessels, rarely seen well in younger normal subjects under these conditions, are seen readily at locations eccentric to the PED. (C) Mid-phase fluorescein angiogram, with a fundus camera, showing hyperfluorescence along the superior margin of the PED, and infero-temporally, which is beneath and obscured by the blood. These hyperfluorescent areas are suspicious for choroidal new vessels CNV. (D) Late-phase fluorescein angiogram. The PED shows irregular filling. As in the mid-phase fluorescein angiogram, there is increased fluorescence along the superior margin of the PED and infero-temporal to the PED, beneath and obscured by the blood. These hyperfluorescent areas are suspicious for CNV. (E) 830 nm image of the same eye, for the direct mode (800 μm aperture) and large field size, showing extensive sub-retinal pathology, some of which is not easily appreciated in (A) and (C–D), the more traditional imaging modes. The location of the PED and blood (the darkened region) are in good agreement with (A–D). There is a region of discontinuity of the pigment epithelium in the vicinity of the PED, seen through the hemorrhage. The area infero-temporal to the PED is suspicious for CNV. The superior margin of the PED is not suspicious for CNV, unlike the fluorescein angiogram. (F) 830 nm image of the same eye, for the indirect mode (400 μm stop) and large field size, showing extensive sub-retinal pathology. Topographic subretinal features are emphasized, such as the accumulation of fluid in the PED, the increased thickness in the region of suspected CNV infero-temporal to the PED. The area containing the fluid, as seen on fluorescein angiography, appears darker, since little light is returning from the deeper layers in this region. Note the irregularities in thickness of the sub-retinal layers, seen especially superior to the PED, consistent with drusen and retinal pigment epithelium pathology. (G) 830 nm image (similar condition to E) 2 months later, showing partial re-absorption of blood. Better contrast of the sub-retinal structures peripheral to the PED is achieved than in (E), since (E) required a greater amount of light to penetrate the blood. (H) 830 nm, small field size, direct mode (400 μm aperture). This magnified and more tightly confocal image emphasizes the superficial aspects of the PED, such as the drusen above the fluid and hyperpigmented regions, as well as detail in the region of the suspected CNV. These imaging conditions allow visualization of features not seen with more traditional imaging methods (A–D).

drusen or fluid accumulation. Indirect mode allowed the discrimination between depigmented regions, such as window defects, from thickened structures, such as drusen. Structures never visualized before *in vivo*, as well as those previously seen only with the use of dye to enhance contrast, can be seen.

Infrared imaging visualizes drusen not detectable either with ophthalmic examination or in a color photograph. Many, but not all, of these were small (10–40 μm). Addtional larger or confluent structures were also seen only with infrared imaging, and these typically were low contrast or were adjacent to or overlapping with large scattering sources, such as soft drusen or regions of atrophy. Given the resolution of our system, drusen < 10 μm cannot be resolved nor can the size of small drusen be measured, although these could be detected given sufficient contrast.

Capillaries in choroidal new vessels or the foveal avascular zone (10 μm) are not resolved without contrast enhancing agents. However, low contrast, larger structures are seen, such as blood-filled membranes or fluid leakage. Thus, choroidal new vessesl are seen not as a group of vessels, but rather as a dark central core with a surrounding whitish region, with the entire complex often appearing structured, thickened, or under traction with striae.

Thick fluid layers or turbid fluid such as in a hemorrhage or a retinal pigment epithelial detachment do not readily transmit light either laterally or to and from deeper layers and appear dark. Other absorbing materials, such as clumped pigment, also appear dark and block light from spreading laterally or to and from deeper layers. These appear darker than surrounding regions, even if contrast enhancing dyes are used. The light level needed to provide useful contrast through thick or turbid fluid must be raised above what produces a good image for the surrounding fundus. In extreme cases, superficial details only were seen. For most sub-retinal structures, however, useful images can be obtained at non-aversive levels in adults or children.

REFERENCES

Assendelft, O. W. (1970). *Spectroscopy of hemoglobin derivatives.* Springfield, IL: C. C. Thomas.

Bartsch, D.-U. & Freeman, W. R. (1994). Axial intensity distribution analysis of the human retina with a confocal scanning laser tomograph. *Experimental Eye Research, 58,* 161–173.

Bonin, P., Faunay, F. & Fauconnier, T. (1990). Notre experience de l'etude clinique de l'oeil dans le domaine du proche infrarouge. *Opttalmologie, 4,* 33–39.

Boulton, M., Docchio, F., Dayhaw-Barker, P., Ramponi, R. & Cubeddu, R. (1990). Age-related changes in the morphology, absorption, and fluorescence of melanosomes and lipofuscin granules of the retinal pigment epithelium. *Vision Research, 9,* 1291–1303.

Bressler, N. M, Bressler, S. B., Seddon, J. M., Gragoudas, E. S. & Jacobsen, L. P. (1988). Drusen characteristics in patients with exudative versus non-exudative age-related macular degeneration. *Retina, 8,* 109–114.

Bressler N. M., Silva J. C., Bressler S. B., Fine S. L. & Green W. R. (1994). Clinicopathologic correlation of drusen and retinal pigment epithelial abnormalities in age–related macular degeneration. *Retina, 14,* 130–142.

Campbell, F. W. & Gubisch, R. W. (1966). Optical quality of the human eye. *Journal of Physiololgy, 186,* 558–578.

Cornsweet, T. N. & Crane, H. D. (1970). Servo-controlled infrared optometer. *Journal of the Optical Society of America 60,* 548–554.

Delori, F. C. & Pflibsen, K. P. (1989). Spectral reflectance of the human ocular fundus. *Applied Optics, 28,* 1061–1077.

Delori F. C., Gragoudas E. S., Francisco R. & Pruett R. C. (1977). Monochromatic ophthalmoscopy and fundus photography: The normal fundus *Archives of Ophthalmolology, 95,* 861–868.

Destro, M. & Puliafito, C. (1989). Indocyanine green videoangiography of choroidal neovascularization. *Ophthalmology, 96,* 846–853.

Ducrey N. M., Delori F. C. & Gragoudas E. S. (1979). Monochromatic ophthalmoscopy and fundus photography: The pathological fundus. *Archives of Ophthalmolology, 97,* 288–293.

Eisner, A., Stoumbos, V. D., Klein, M. L. & Fleming, S. (1991). Relations between fundus appearance and function. *Investigative Ophthalmology and Visual Science, 32,* 8–20.

Elsner, A. E., Burns, S. A. & Webb. R. H. (1988). Photopigment densitometry with a scanning laser ophthalmoscope. *Optical Society of America Technical Digest, 11,* WY3.

Elsner, A. E., Burns, S. A., Delori, F. C. & Webb, R. H. (1990). Quantitative reflectometry with the SLO. In Nasemann, J. E. & Burk, R. O. W. (Eds), *Laser scanning ophthalmoscopy and tomography* (pp. 109–121). New York: Quintessenz-Verlag.

Elsner, A. E., Burns, S. A., Hughes, G. W. & Webb, R. H. (1990). Evaluating the photoreceptor/rpe complex with and SLO, *Noninvasive Assessment of the Visual System, Technical Digest, Optical Society of America, 3,* 40–43.

Elsner, A. E., Burns, S. A., Kreitz, M. R. & Weiter, J. J. (1991). New views of the retina/RPE complex: quantifying sub-retinal pathology. *Noninvasive Assessment of the Visual System, Technical Digest, Optical Society of America, 1,* 150–153.

Elsner, A. E., Burns, S. A., Hughes, G. W. & Webb, R. H. (1992a). Reflectometry with a scanning laser ophthalmoscope. *Applied Optics, 31,* 3697–3710.

Elsner, A. E., Burns, S. A. & Weiter, J. J. (1992b). Retinal densitometry in retinal tears and detachments. *Clinical Vision Sciences, 7,* 489–500

Elsner, A. E., Jalkh, A. E. & Weiter, J. J. (1993). New devices in retinal imaging and functional evaluation. In Freeman, W. (Ed.) *Practical atlas of retinal disease and therapy* (pp. 19–35). New York: Raven.

Elsner A. E., Staurenghi G., Weiter J. J., Buzney S. M., Wolf, S. & Wald, K. J. (1993). Infrared imaging in age related macular degeneration: retinal pigment epithelial detachments. *Noninvasive Assessment of the Visual System, Technical Digest, Optical Society of America, 3,* 232–235.

Fausset, T. M. & Enoch, J. M. (1987). A rapid technique for kinetic visual field determination in young children and adults with central retinal lesions. *International Perimetric Society Documents on the Ophthalmological Proceedings Series, 49,* 495–501.

Feeney-Burns, L. & Ellersieck, M. R. (1985). Age-related changes in the ultrastructure of Bruch's membrane. *American Journal Ophthalmology, 100,* 686–697.

Flower, R. W. & Hochheimer, B. F. (1973). A clinical technique and apparatus for simultaneous angiography of the separate retinal and choroidal circulations. *Investigative Ophthalmology, 12,* 248–261.

Gabel, V.-P., Birngruber, R. & Hillenkamp. F. (1978). Visible and near infrared light absorption in pigment eipthelium and choroid. In Shimuzu, K. & Osterhuis, J. A. (Ed.) *XXIII Concilium Ophthalmology Kyoto* (pp. 658–662) Amsterdam-Oxford: Exerpta Medica.

Green, W. R. & Enger, C. (1993). Age-related macular degeneration histopathologic studies. *Ophthalmology, 100,* 1519–1535.

Jaeger W., Gotz M. L. & Blankenagel A. (1986). Lasst sich mit Hilfe der Infrarot-Photographie etwas uber die Prognose der hereditaren Makuladegenerationen aussagen? *Klinische Monatblaetter der Augenheilkunde, 188,* 178–181.

Leibowitz, H., Kruger, D. E., Maunder, L. R., Milton, R. C., Kini, M. M., Kahn, H. A., Mickerson, R. J., Pool, J., Colton, T. L., Ganley, J. P. & Loewenstein, J. (1980). The Framingham Eye Study

Monograph: an ophthalmological and epidemiological study of cataract, glaucoma, diabetic retinopathy, macular degeneration, and visual acuity in a general population of 2631 adults, 1973–1975. *Survey of Ophthalmology*, *24* (Suppl.), 335–610.

Menon, I. A., Persad, S., Haberman, H. F., Kurian, C. J. & Basu, P: K. (1982). A qualitative study of the melanins from blue and brown eyes. *Experimental Eye Research*, *34*, 531–537.

van Norren, D. & Tiemeijer, L. F. (1986). Spectral reflectance of the human eye. *Vision Research*, *26*, 313–320.

Pokorny, J., Smith, V. C. & Lutze, M. (1987). Aging of the human lens. *Applied Optics*, *26*, 1437–1440.

Sarks, J. P., Sarks, S. H. & Killingsworth, M. C. (1988). Evolution of geographic atrophy of the retinal pigment epithelium. *Eye*, *2*, 552–577.

van der Schaft, T. L., Mooy, C. M., de Bruijn, W. C., Oron, F. G., Mulder, P. G. H. & de Jong, P. T. V. M. (1992). Histologic features of the early stages of age-related macular degeneration. *Ophthalmology*, *99*, 278–286.

Scheider, A., Kaboth, A. & Neuhauser, L. (1992). Detection of sub-retinal neovascular membranes with indocyanine green and an infrared scanning laser ophthalmoscope. *American Journal of Ophthalmology*, *113*, 45–51.

Sebag, M., Peli, E. & Lahav, M. (1991). Image analysis of changes in drusen area. *Acta Ophthalmologica*, *69*, 603–610.

Slayter, E. M. & Slayter, H. S. (1992). *Light and electron microscopy* (pp. 124–125). Cambridge: Cambridge University Press.

Snodderly, D. M., Brown, P. K., Delori, F. C. & Auran, J. D. (1984). The macular pigment. I. Absorbance spectra, localization, and discrimination from other yellow pigments in primate retinas. *Investigative Ophthalmology and Visual Sciences*, *25*, 660–673.

Sullivan, S. A. (1963). Absorption in distilled, sea, and heavy water. *Journal of the Optical Society of America*, *53*, 962–968.

Sunness, J. S., Johnson, M. A., Massof, R. W. & Marcus, S. (1988). Retinal sensitivity over drusen and nondrusen areas. *Archives of Ophthalmology*, *106*, 1081–1084.

Webb, R. H. & Delori, F. C. (1988). How we see the retina. In Marshall, J. (Ed.) *Laser technology in ophthalmology* (pp. 3–14). Amsterdam: Kugler & Ghedini.

Webb, R. H., Hughes, G. W. & Delori, F. C. (1987). Confocal scanning laser ophthalmoscope. *Applied Optics*, *26*, 1492–1499.

Weiter, J. J., Delori, F. C., Wing, G. L. & Fitch, K. F. (1986). Retinal pigment epithelium lipofuscin and melanin and choroidal melanin in human eyes. *Investigative Ophthalmololgy and Visual Science*, *27*, 145–152.

Wolbarsht, M. L., Walsh, A. W. & George, G. (1981). Melanin, a unique biological absorber. *Applied Optics*, *20*, 2184–2186.

Wyszecki G. & Stiles W. S. (1982a). *Color science* (pp. 101–102). New York: Wiley.

Wyszecki G. & Stiles W. S. (1982b). *Color science* (pp. 105–107). New York: Wiley.